Dynamic Response and Relative Sensitivity of Vanadium In-Core Flux Detectors and Lead-cables in Pt. Lepreau

by

B. Sur[1], G. Gomes[2], J. Handbury[3], C.W. Newman[4], and E.G. Young[4]

Abstract

The Pt. Lepreau core-monitoring group has developed a program[5] to use the signals from vanadium in-core flux detectors to accurately map the flux and power distribution inside the core, in real time, including periods of reactor power transients. In order to construct an accurate real-time flux map, the vanadium detector signals, which have a dominant (~ 93%) delayed component, have to be dynamically compensated; and the signal contribution from the lead-cable, which amounts to approximately 25% of the prompt detector signal, has to be properly accounted for. Data from vanadium detectors was acquired during a recent run-down test in order to assess the detector and lead-cable response parameters to be used in the dynamic compensation and flux-mapping algorithms. The run-down data for individual detectors exhibit systematic variations in the values of prompt fraction and amplitudes for delayed terms. A statistical analysis of the distributions of these amplitudes allows the separation of dynamic response terms due to the lead-cable and the detector itself. An average value for the relative sensitivity (compared to the detector) of the lead-cable is also extracted. This paper presents the methodology and the results of analyzing the run-down test data from the vanadium flux-mapping detectors at Pt. Lepreau.

Funding for this work was provided by New Brunswick Power Commission and by Atomic Energy of Canada Ltd.

Introduction

In-Core Flux Detectors (ICFDs) with vanadium emitters are used in the Pt. Lepreau Generating Station (PLGS) CANDU 6 class reactor core for flux-mapping. 102 such vanadium ICFDs of the Straight Individually Replaceable (SIR) design are installed in 22 vertical flux-detector assemblies (VFDs). The neutron-induced signal from the vanadium emitter is transmitted out of the core via inconel 600 lead-cables. The in-core portion of

[1] AECL, Chalk River Laboratories, Chalk River, Ontario K0J 1J0.
[2] AECL, Sheridan Park Research Community, Mississauga, Ontario L5K 1B2.
[3] Atlantic Nuclear Services, Fredricton, New Brunswick.
[4] NB Power, Pt. Lepreau GS, Pt. Lepreau, New Brunswick E0G 2H0.
[5] C. Newman, "Technical Specification for MICROMAP: A Powermapping and Compliance Monitoring Program", PLGS TS-66504 (1997).

the lead-cable produces a small but significant fraction (approximately 1% to 3% in a steady-state neutron flux) of the total signal output of each ICFD. The lead-cable signal contribution is proportional to the lead-cable relative sensitivity and to the neutron flux integrated over the in-core length of the lead-cable. Signals from ICFDs which are lower in the core (longer lead-cable) are therefore systematically larger than those from the top of the core. If not corrected for the lead-cable contribution, these signals give rise to a systematic top-to-bottom tilt in the computed steady-state flux-map.

The PLGS Micromap program[5] computes an instantaneous, rather than steady-state flux map using time-corrected (i.e. dynamically compensated) vanadium ICFD signals. The dynamic compensation scheme uses knowledge of the ICFD dynamic response to extract the prompt component of the signal. The dynamic response of a vanadium ICFD to a change in neutron flux consists of an approximately 7% prompt response (prompt fraction, Pf) plus a dominant first order lag term with a 325 s time-constant. The lead-cable signal by itself, on the other hand, has a 150% to 200% prompt fraction and a dominant 3.7 h lag term. The lead-cable signal contribution is thus further increased in the dynamically compensated (i.e. prompt component) of the total ICFD signal.

As the ICFDs age in the core, the neutron sensitivity and dynamic response parameters of both the vanadium emitter and of the lead-cable change due to burn-up (neutron-induced transmutation of constituent isotopes). The burn-up dependence of the signals from the 99.75% mono-isotopic vanadium emitter is well-known, but that of the lead-cable (and ICFD sheath), due to poly-isotopic inconel 600, is vastly more complicated, and not well understood. Therefore, in order to construct an accurate, instantaneous flux-map, it is necessary to measure and separate, in-situ, the relative magnitude and the dynamic response of the signal component due to the lead-cable from that due to the vanadium ICFD itself.

An approach towards this goal, based on analysis of data from vanadium ICFD responses to a manual run-down test in PLGS is described in this paper.

Data

The data referred to in this paper was acquired for a 24 h period prior to, and following a manual Shut-Down System 1 (SDS1) run-down test at PLGS in1997 November. The reactor power was first reduced from 100% full-power (FP) to 77% FP to unload the turbines. About 2600 minutes after the power reduction, the reactor was tripped manually, resulting in a rapid (about 1 s duration) power and flux reduction due to the insertion of shut-off rods (SORs) into the core.

Data from 17 of the 102 flux-mapping vanadium ICFDs, 14 zone-control platinum-clad inconel ICFDs and 3 ion-chambers (ICs) was acquired at 100 ms intervals via the Fast Trend Log (FTL) in the PLGS Digital Control Computers (DCCs). Data from all the safety and control system platinum-clad ICFDs, ICs, and reactivity control devices - liquid zone controllers (LCZs), Adjuster rods, Mechanical Control Absorbers (MCAs) and the SORs - was automatically acquired on the plant High Speed Data Logger (HSDL) at a sampling period of 50 ms, for a 5 minute period preceding and following the reactor trip. Continuous plant data, from all sensors, was available at 6 s intervals from the DCCs, the HSDL, and the safety system monitoring computer (SSMC).

The vanadium ICFD response data, along with data from other sensors, was extracted from the various data sources, correlated, corrected, and analyzed. The data extraction and correction procedures are described in detail in an accompanying paper in these proceedings[6].

The flux distribution in the core, during and after SOR insertion, was also simulated via the Reactor Fueling Simulation Program (RFSP)[7]. The time history of the simulated fluxes at individual detector sites were subsequently used in the data analysis to characterize the individual ICFD dynamic response parameters.

The measured response of one of the ion chambers, along with the RFSP-simulated flux at the ion-chamber site, are shown for the first few seconds following the trip, in Figure 1. The responses in Figure 1 have been normalized to the reading just prior to the trip. The normalized flux seen by the ion-chamber is expected to approximate the average normalized flux in the reactor core. The agreement between the simulated flux and the measured ion-chamber signal (expected to be 100% prompt-responding) is good. The flux in the core decreases to approximately 5% of its initial value within 1.5 s of SOR insertion.

A sample of normalized, measured responses from three vanadium ICFDs located in assembly VFD02, at three different vertical locations inside the core - denoted from top to bottom as RE3, RE5, and RE7 - are shown in Figure 2. RFSP-simulated fluxes at these detector-sites are shown in Figure 3.

The vanadium ICFD responses in Figure 2 indicate that the magnitude of their prompt response, i.e., their "prompt fraction" is approximately 7%. The dominant 325 s delayed response is also evident. A comparison of Figure 2 and Figure 3 shows two other systematic effects. The first is due to the finite time taken by the SORs to travel from the top to the bottom of the core. Both the simulated fluxes and the measured responses indicate that the ICFDs which are lower in the core experience the rapid decrease in flux at a slightly later time than ICFDs which are higher in the core (the approximately step decrease in ICFD response and in the ICFD-site simulated flux occurs later in time). The second effect is due to the lead-cable contribution to the total ICFD signal. ICFDs which are lower in the core (longer lead-cables) appear to have a distinctly larger "step-size" or

[6] G. Gomes: "MDRAP - a MATLAB-based Detector Response Analysis Package", these proceedings.

[7] B. Rouben: "Overview of Current RFSP-code Capabilities for CANDU Core Analysis", AECL-11047, 1998 January.

prompt response following the trip, even though the step-size of the simulated fluxes at all three ICFD sites are approximately equal.

The first of the above effects - the transient flux-shape distortion in the core due to the SOR flight time - is an example of a phenomenon which has to be correctly accounted for in order to accurately assess the ICFD dynamic response parameters. The second effect - the systematic dependence of the ICFD dynamic response parameters on the lead-cable length - is used in the following analysis to extract the lead-cable relative sensitivity and to separate the lead-cable and vanadium dynamic responses.

Analysis

Following the acquisition and extraction of detector and device position data, and the RFSP-simulation of fluxes at the detector sites, the data analysis proceeded in two steps. The first step was the characterization of the dynamic response of individual vanadium detectors. The second was a global analysis of all the dynamic response parameters as a function of lead-cable-dependent parameters (the integrated lead-cable fluxes) in order to separate the average dynamic response of the vanadium emitters from that of the lead-cables, and to deduce the average lead-cable relative sensitivity.

Characterization of individual ICFD dynamic responses

The dynamic response of ICFD signals to a change in neutron flux (i.e. the ICFD transfer function) is parameterized by a prompt fraction, Pf, plus a sum of first-order lags, with amplitudes, a_i, and time-constants, τ_i, where the subscript, i, refers to the individual lag terms. Details of the mathematical formulation of the parameterized detector response are given in the Appendix. Characterization of individual ICFD dynamic response parameters starts with a "reference" or time-varying "input" flux. This flux is processed through the ICFD response model, and the model output is compared to the measured ICFD response. The parameters in the model are varied to obtain the best fit to the measured response. The program MDRAP[6] was used to carry out the parameter fitting process. Only the amplitudes of the lag terms were varied, while the time-constants were fixed, as described below. The detector electronics loop parameters (response times) were assumed known, and not varied. For the vanadium ICFD analysis, an ICFD response model in Laplace or s-space was used in MDRAP. Consequently, the non-equilibration of long-lived lag terms due to the flux-history prior to the trip was not accounted for in this analysis.

Reference fluxes

Two sources of reference flux were used in MDRAP. The first was the measured, normalized flux in one of the ion-chambers (channel C). This provides a direct measure of the neutron flux sources in the reactor-core, including delayed and photo- neutrons, but does not account for the transient flux distortions caused by the SOR flight-time. However, as explained in the Appendix, the discrepancies due to the SOR flight-time are expected to be small in the case of vanadium ICFDs, because the time-scale associated with this effect (less than 1 s) is small compared to the dominant 325 s time constant of the vanadium emitter signal. The time lags due to the electronics loop for the IC are similar to those for the ICFDs, hence the electronics are ignored for this reference flux.

The second reference flux used was the RFSP simulated ICFD-site flux for individual detectors. This simulated flux takes the SOR flight-time-induced flux-shape distortions into account. However, there are timing problems in synchronizing the exact start-time and rate of SOR insertion, between the RFSP simulation and the actual data. Also, the RFSP flux simulations were limited to 600 s following SOR insertion, whereas the detector responses were acquired and fitted for more than 12 hours following the trip. This necessitated the use of an assumed linear decrease in flux from the last RFSP-calculated value to zero flux at the last acquired data point. Finally, in this particular case, the RFSP simulated fluxes were pre-calculated using typical reactivity device positions before and during the trip, as opposed to measured positions. Nevertheless, as shown in Figures 1, 2 and 3, the RFSP-simulated fluxes show very good qualitative agreement with measured detector-site fluxes (after ICFD dynamics are taken into account). The detector loop electronics response times were included in the model[6] when the RFSP-simulated reference flux was used.

Choice of time constants

Vanadium SIR in-core flux detectors have a vanadium core-wire or emitter, MgO mineral insulation and an inconel 600 sheath. The lead-cables, which also produce a small signal contribution, have inconel 600 cores and sheaths, and MgO insulation. All the delayed signal contributions will therefore, in principle, be due to beta-decaying nuclei produced by neutron transmutation of vanadium and of the elements in inconel 600 alloy.

Neutron capture in vanadium produces ^{52}V which beta-decays with a half-life of 3.76 m or a mean-life of 325 s (= 3.76m / ln 2). Thus the dominant delayed component of current in vanadium ICFDs has a time-constant of 325 s. This positive delayed current component is produced by the ICFD emitter only.

Inconel 600 is an alloy, composed primarily of nickel (approximately 74% by weight), chromium (approximately 14%), iron (approximately 8%) plus small amounts of several other elements such as manganese, silicon, cobalt etc. The primary beta-decaying nuclei, produced by neutron transmutation are expected to be ^{65}Ni ($t_{1/2}$ = 2.52 h) and ^{56}Mn ($t_{1/2}$ = 2.58 h). Thus the major delayed component of current produced by inconel 600 has a time constant of approximately 3.7 h (= 2.55 h / ln 2). This negative delayed current component (due to charge transfer predominantly from sheath to core) is produced by both the detector and the lead-cable.

Dynamic response analyses of inconel-emitter ICFDs have shown that there are other delayed components also present in the inconel 600 response. Individual detectors and lead-cables show different values of the dominant time constants for these residual delayed currents. These time constants cannot, in general, be identified with the mean life of any particular beta-decaying isotope. It has been speculated that some of these residual terms may be due to charge hold-up (electron traps) in the MgO insulator[8, 9]. Based on analyses of a number of inconel-emitter ICFDs, design time-constant values of 95 s, 25.6 m and 46 to 95 h have been chosen for these residual terms[8, 9].

As the detectors age or burn up, the concentration of parent nuclides change, and the amplitudes of these individual delay terms in the detector response will also change. The time constant values of 325 s and the 3.7 h will however remain constant since they can be identified with specific beta-decaying nuclei. It is less certain whether the other adopted time-constant values remain unchanged with burn-up. This is because these values are weighted averages, and the weights may change due to burn-up. Also, charge trapping effects in the MgO insulation, if present, will be significantly affected by neutron irradiation.

Due to the above considerations, the vanadium ICFD response data was first fitted with a response function consisting of a prompt fraction, two delayed terms with 325 s and 3.7 h time-constants, and a constant term to account for any residual dc-offsets in the detector electronics or the presence of any extremely long lags, due to the build-up of very long-lived β-emitting isotopes. Results of these fits are reported in the following section.

Subsequently, lag terms with time-constants of 25.6 m and 95 s were also added to the fitted response. These time constants are less than a factor of 5 different from the dominant 325 s time-constant. Consequently, adding these terms to the ICFD dynamic response model gave inconsistent results. For instance the best-fit amplitudes derived from the two reference fluxes disagreed significantly. The amplitude for the 325 s term changed significantly, contrary to expectations. The SOR flight-time effect was absorbed by the shortest time-constant - in this case 95 s - and masked the effect due to the lead-cable. Due to these inconsistencies, the amplitudes fit by the "extended" model (using the 25.6 m and 95 s time-constants in addition to the "standard" 325 s and 3.7 h terms) are not further discussed in this paper.

---

[8] C.J. Allan, "Review of the Dynamic Response of Self-Powered Flux Detectors in CANDU Reactors", Proc. 2nd Annual Conf. Of CNS, Ottawa, 1981 June.

[9] C.J. Allan, N.H. Drewell, and D.S. Hall, "Recent Advances in Self-Powered Flux Detector Development for CANDU Reactors", IAEA-SM-265/8, 1982.

Results of vanadium detector dynamic response characterization

The best-fit amplitudes of the 325 s and 3.7 h lag terms, the value of the constant (dc-offset term), the calculated prompt fraction and the 1-σ error for each of these parameters are shown for each vanadium detector in Table 1 and Table 2. Table 1 shows the results from using the IC flux as a common reference for all detectors, while Table 2 shows the results from using the RFSP-simulated ICFD-site fluxes plus electronics, as the reference flux for individual detectors. There are small discrepancies between the two cases.

Note that there is no correction for the pre-trip power maneuvering in these fitted amplitudes. The MDRAP model used for these fits assumes that all lag terms have equilibrated prior to the trip. However, there was significant power maneuvering prior to the particular SDS1 trip analyzed here - in particular the power was reduced from 100% to approximately 77%, about 2600 minutes before the trip. Thus the longer lived delay terms, particularly the 3.7 h term is not expected to have equilibrated. The degree of non-equilibration for each delay term is calculated separately (as explained in the accompanying paper by G. Gomes[6]) by MDRAP, using the pre-trip response of nearby platinum-clad inconel ICFDs to estimate the local flux history for each vanadium ICFD. This pre-trip correction has not yet been applied in the vanadium detector analysis.

Separation of vanadium ICFD and lead-cable responses and the lead-cable relative sensitivity.

The dynamic response parameters of the vanadium ICFDs plus lead-cables, as obtained above, were collectively analyzed, under assumptions listed below, in order to separate the response of the average detector from the average lead-cable segment; and to derive the lead-cable relative sensitivity. Details of the derivation of the dynamic response model used for detector plus lead-cable are given in the Appendix. As shown in Figure 4, since the vanadium emitters are each one CANDU lattice pitch (28.57 cm) in length, the detector plus lead-cable is modeled as a collection of one-lattice pitch long current-generating segments, connected in series. The segments are labeled by the index, j. j = 0 denotes the detector segment, and j = 1 to n denote the lead-cable segments for a n-lattice-pitch-long lead-cable.

Assumptions and additional data sources used in the analysis are listed below:

1. It is assumed that all the detector segments (j=0) have a standard steady-state or dc sensitivity, S_0. The initial sensitivity of individual detectors is calibrated during manufacture and installation, and the decrease in sensitivity due to burn-up of ^{51}V is tracked at PLGS, by accumulating the mapped flux at each detector site as a function of detector age. Individual detector sensitivities are thus obtained by dividing the

standard sensitivity by a factor. This factor is tabulated in the "$1/S_{ICFD}$" column of Table 3.

2. It is assumed here that all the lead-cable segments have the same dc sensitivity, S_{LC}. Although it is anticipated that the sensitivity of individual lead-cable segments will vary according to their burn-up history, a previous study[10] has shown that the lead-cable sensitivities do not follow the predicted trend. Empirically, the lead-cables seem to have a constant, lower-than-predicted dc sensitivity after an in-core exposure of roughly 300 effective full-power days (FPD). Improved statistics from run-down data of additional vanadium ICFDs may allow the unfolding of burn-up or flux-dependent lead-cable segment sensitivities in the future.

3. It is assumed that all the detectors have the same dynamic response parameters, characterized by amplitude a_{0i} for the lag term i. In reality, detector dynamic response parameters would be expected to vary slightly with individual detector burn-up.

4. It is assumed that all lead-cable segments have the same dynamic response parameters, characterized by amplitude a_{LCi} for the lag term i. As for the detectors, lead-cable dynamic response parameters would be expected to vary slightly with burn-up.

5. It is assumed that in the lead-cable dynamic response, the amplitude for the 325 s lag term, $a_{LC\ 325\ s}$, is zero. This assumption is justified because the lead-cable composition (inconel 600) does not contain ^{51}V, the isotope which produces the 325 s lag term. This assumption provides a powerful constraint in separating the lead-cable response from the vanadium detector response, and in deriving the lead-cable relative sensitivity, α_{LC}.

6. The ratio of the integrated lead-cable flux to the detector-site flux is required for this analysis. The flux at the individual detector sites, and the sum of the fluxes at all the lead-cable segment-sites for the corresponding detector, were obtained from the steady-state RFSP "production" run at PLGS for the time-period just prior to the trip test. These quantities, and their ratio, "$\Sigma\beta_{LC}$" are shown in columns 3, 4 and 5 of Table 3 respectively.

The results of the global analysis are given in Table 4. There are two sets of results: one for the MDRAP-derived amplitudes using the ion chamber as the reference flux, and the other for the MDRAP-derived amplitudes using the RFSP-simulated detector-site fluxes as reference. The data-points, i.e., the MDRAP-derived amplitudes, and the fitted curves are shown for each case in Figure 5 and Figure 6 respectively.

---

[10] B. Sur, D.P. McAllindon and C.M. Bailey: "Investigation into Anomalous Vanadium SIR Lead-cable Responses in Pt. Lepreau and Gentilly-2", Proceedings of the 18th Annual CNS Conf., Toronto, 1997 June.

Discussion

The general features of the detector plus lead-cable model derived in the Appendix are reflected in the data - there is a systematic variation in all the MRAP-derived dynamic response amplitudes versus the lead-cable integrated flux (Figure 5 and Figure 6).

The results for the average detector amplitudes agree fairly well between the two reference fluxes (Table 4). The lead-cable parameters derived from the two sets of reference flux do not agree within the derived error bars. There is general agreement in the trend of the lead-cable dynamic response parameters - the delayed amplitudes are negative and the prompt response is greater than one, i.e. "over-prompt" in both cases. These features are also consistent with previous studies of lead-cable dynamic response.

The values of the average lead-cable relative sensitivity derived from two references fluxes (α_{LC} in Table 4) differ by almost a factor of 2. The value derived from the RFSP-simulated reference flux - $\alpha_{LC} = 0.056\%$ - is close to the originally predicted value of 0.047%, while that derived from the IC reference flux - $\alpha_{LC} = 0.024\%$ - is close to the value of about 0.035% recommended as the result of a study[10] of the response of detector-less lead-cables installed in PLGS and in Gentilly-2.

The cause of the discrepancy between the lead-cable results from the two reference fluxes is not clear at this stage of the analysis. It is important to either validate or eliminate as many of the assumptions made in deriving the present results as possible. Eliminating the effect due to the pre-trip power maneuvering is considered the most significant of the assumptions that can be reduced by improved analysis. The most significant source of uncertainty at present is the scatter in the data - i.e. in the amplitudes of individual detectors vs. the lead-cable integrated flux. Thus the largest improvement overall in deriving the lead-cable relative sensitivity using this methodology would be expected to result from using trip-response data from a large number of (the 102 installed) vanadium detectors in the PLGS core.

Table 1: MDRAP-optimized delay-term amplitudes for vanadium ICFDs (plus lead-cables), using the measured Ion Chamber C response as the reference flux.

Detector	325 s	3.7 h	dc-offset	Prompt fraction
VFD01-RE3C	0.9348 ± 0.0004	-0.0094 ± 0.0004	-0.0004 ± 0.0002	0.0746 ± 0.0008
VFD01-RE6A	0.9317 ± 0.0004	-0.0110 ± 0.0004	0.0002 ± 0.0002	0.0793 ± 0.0007
VFD02-RE3A	0.9350 ± 0.0007	-0.0084 ± 0.0007	-0.0013 ± 0.0003	0.0734 ± 0.0014
VFD02-RE5B	0.9354 ± 0.0003	-0.0113 ± 0.0003	0.0000 ± 0.0002	0.0759 ± 0.0006
VFD02-RE7A	0.9267 ± 0.0005	-0.0104 ± 0.0005	0.0002 ± 0.0002	0.0837 ± 0.0010
VFD03-RE3A	0.9335 ± 0.0004	-0.0092 ± 0.0004	-0.0004 ± 0.0002	0.0757 ± 0.0007
VFD03-RE6C	0.9353 ± 0.0005	-0.0125 ± 0.0004	0.0002 ± 0.0002	0.0772 ± 0.0008
VFD24-RE6A	0.9330 ± 0.0004	-0.0119 ± 0.0004	0.0003 ± 0.0002	0.0789 ± 0.0008
VFD25-RE3C	0.9373 ± 0.0007	-0.0097 ± 0.0007	-0.0013 ± 0.0003	0.0724 ± 0.0013
VFD25-RE5B	0.9345 ± 0.0003	-0.0111 ± 0.0002	-0.0002 ± 0.0002	0.0766 ± 0.0005
VFD26-RE6C	0.9368 ± 0.0004	-0.0127 ± 0.0003	-0.0001 ± 0.0002	0.0759 ± 0.0007
VFD11-RE4C	0.9282 ± 0.0005	-0.0147 ± 0.0004	0.0001 ± 0.0002	0.0865 ± 0.0009
VFD12-RE2A	0.9339 ± 0.0005	-0.0121 ± 0.0004	-0.0006 ± 0.0002	0.0782 ± 0.0008
VFD12-RE6A	0.9326 ± 0.0004	-0.0132 ± 0.0003	0.0000 ± 0.0002	0.0806 ± 0.0007
VFD14-RE8C	0.9264 ± 0.0004	-0.0131 ± 0.0005	0.0001 ± 0.0002	0.0867 ± 0.0009
VFD15-RE3B	0.9337 ± 0.0005	-0.0125 ± 0.0004	-0.0007 ± 0.0002	0.0788 ± 0.0009
VFD16-RE4C	0.9365 ± 0.0005	-0.0192 ± 0.0004	-0.0004 ± 0.0002	0.0827 ± 0.0009

Table 2: MDRAP-optimized delay-term amplitudes for individual vanadium ICFDs (plus lead-cables), using RFSP-simulated ICFD-site fluxes plus electronics.

Detector	325 s	3.7 h	dc-offset	Prompt fraction
VFD01-RE3C	0.9333 ± 0.0005	-0.007 ± 0.0005	-0.0007 ± 0.0002	0.0737 ± 0.0010
VFD01-RE6A	0.9272 ± 0.0005	-0.007 ± 0.0005	-0.0010 ± 0.0002	0.0798 ± 0.0011
VFD02-RE3A	0.9353 ± 0.0005	-0.007 ± 0.0005	-0.0009 ± 0.0002	0.0717 ± 0.0011
VFD02-RE5B	0.9334 ± 0.0006	-0.008 ± 0.0006	-0.0008 ± 0.0002	0.0746 ± 0.0012
VFD02-RE7A	0.9221 ± 0.0005	-0.006 ± 0.0005	-0.0012 ± 0.0002	0.0840 ± 0.0011
VFD03-RE3A	0.9320 ± 0.0005	-0.007 ± 0.0005	-0.0007 ± 0.0002	0.0748 ± 0.0010
VFD03-RE6C	0.9308 ± 0.0005	-0.009 ± 0.0005	-0.0009 ± 0.0002	0.0777 ± 0.0010
VFD24-RE6A	0.9280 ± 0.0006	-0.008 ± 0.0006	-0.0011 ± 0.0003	0.0796 ± 0.0012
VFD25-RE3C	0.9376 ± 0.0005	-0.008 ± 0.0005	-0.0009 ± 0.0002	0.0706 ± 0.0011
VFD25-RE5B	0.9324 ± 0.0005	-0.008 ± 0.0005	-0.0010 ± 0.0002	0.0755 ± 0.0010
VFD26-RE6C	0.9324 ± 0.0005	-0.009 ± 0.0004	-0.0012 ± 0.0002	0.0764 ± 0.0009
VFD11-RE4C	0.9226 ± 0.0007	-0.010 ± 0.0006	-0.0014 ± 0.0003	0.0873 ± 0.0012
VFD12-RE2A	0.9330 ± 0.0006	-0.010 ± 0.0005	-0.0009 ± 0.0002	0.0765 ± 0.0011
VFD12-RE6A	0.9292 ± 0.0006	-0.009 ± 0.0006	-0.0012 ± 0.0002	0.0800 ± 0.0011
VFD14-RE8C	0.9214 ± 0.0007	-0.008 ± 0.0006	-0.0014 ± 0.0003	0.0870 ± 0.0013
VFD15-RE3B	0.9329 ± 0.0005	-0.010 ± 0.0005	-0.0009 ± 0.0003	0.0771 ± 0.0011
VFD16-RE4C	0.9311 ± 0.0006	-0.015 ± 0.0006	-0.0019 ± 0.0003	0.0835 ± 0.0012

Table 3: Data for individual detectors and lead-cables used to separate vanadium ICFD and lead-cable dynamic responses, and to extract the average lead-cable relative sensitivity.

Detector	$1/S_{ICFD}$*	Det Flux $[cm^{-2}s^{-1}]$	LC Flux $[cm^{-2}s^{-1}]$	$\Sigma\beta_{LC}$ (LC Flux/Det Flux)	$\Sigma\beta_{LC}/S_{ICFD}$
VFD01-RE3C	1.113	2.07E+14	9.05E+14	4.38	4.88
VFD01-RE6A	1.091	2.08E+14	2.66E+15	12.83	14.00
VFD02-RE3A	1.114	2.26E+14	9.13E+14	4.04	4.50
VFD02-RE5B	1.107	2.29E+14	2.32E+15	10.16	11.25
VFD02-RE7A	1.095	2.25E+14	3.73E+15	16.55	18.12
VFD03-RE3A	1.076	1.98E+14	9.51E+14	4.80	5.17
VFD03-RE6C	1.072	2.14E+14	2.74E+15	12.80	13.72
VFD24-RE6A	1.079	2.12E+14	2.74E+15	12.91	13.92
VFD25-RE3C	1.097	2.22E+14	8.86E+14	4.00	4.38
VFD25-RE5B	1.104	2.25E+14	2.25E+15	10.02	11.06
VFD26-RE6C	1.095	2.15E+14	2.80E+15	13.01	14.25
VFD11-RE4C	1.059	2.43E+14	5.55E+15	22.84	24.19
VFD12-RE2A	1.125	3.11E+14	2.38E+15	7.67	8.63
VFD12-RE6A	1.135	3.01E+14	4.18E+15	13.87	15.74
VFD14-RE8C	1.137	3.27E+14	5.64E+15	17.26	19.62
VFD15-RE3B	1.127	3.03E+14	2.37E+15	7.83	8.82
VFD16-RE4C	1.057	2.24E+14	5.62E+15	25.08	26.51

*Note: These are detector relative sensitivity factors (unit-less) which vary from detector to detector due to differences in burn-up and initial calibration. The standard value of new SIR vanadium ICFD sensitivity is divided by these values to obtain the correct individual detector sensitivity.

Table 4: Results of applying the methodology to separate average vanadium ICFD from average lead-cable dynamic response, and to extract the lead-cable average relative sensitivity.

Delayed Term:	325 s	3.7 h	dc-offset	Prompt fraction
Ion Chamber used as reference flux:				
$a_{detector}$	0.9363 ± 0.0007	-0.0078 ± 0.00011	$-6.3E-04 \pm 2E-05$	0.0721 ± 0.0005
a_{LC}	0	-1.38 ± 0.35	0.146 ± 0.023	2.24 ± 0.32
α_{LC}	$2.35E-04 \pm 5.5E-05$			
RFSP-simulated detector-site fluxes used as reference flux:				
$a_{detector}$	0.9369 ± 0.0006	-0.0065 ± 0.00011	$-5.4E-04 \pm 1.7E-05$	0.0701 ± 0.0005
a_{LC}	0	-0.28 ± 0.04	-0.073 ± 0.010	1.35 ± 0.05
α_{LC}	$5.57E-04 \pm 5.5E-05$			

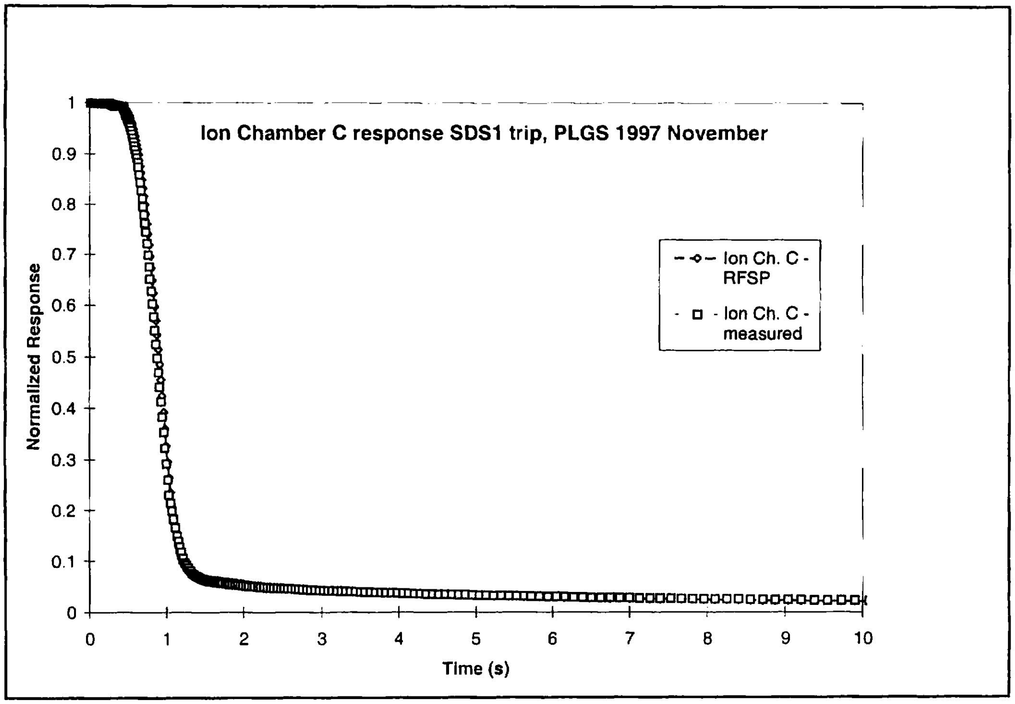

Figure 1: RFSP-simulated, and measured flux run-down signal for Ion Chamber C from the SDS1 trip at PLGS.

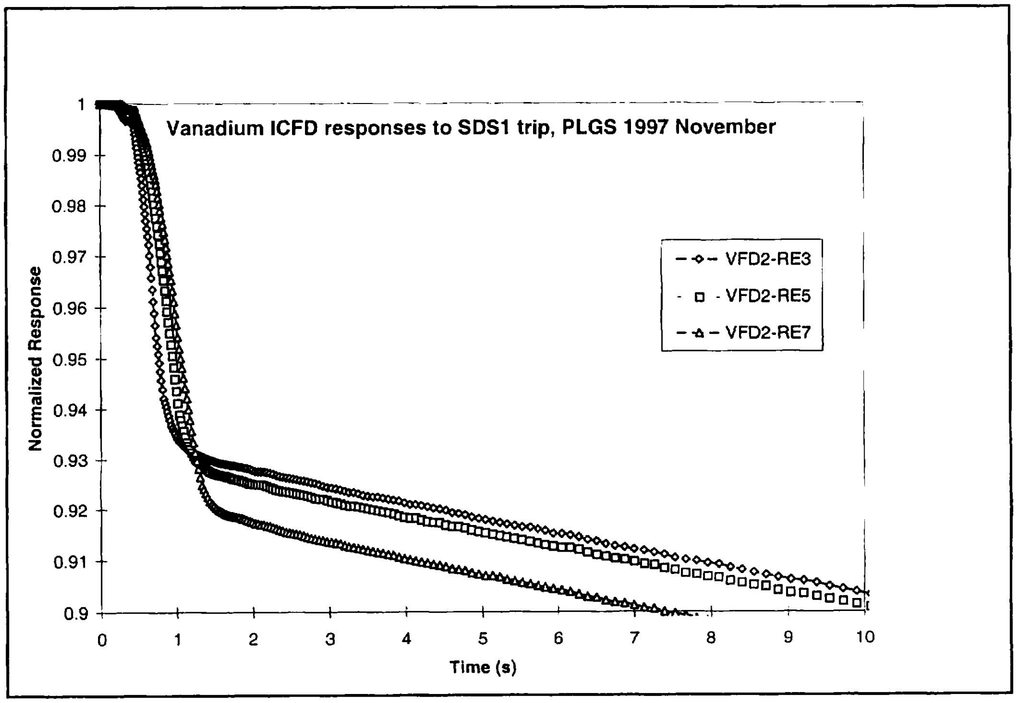

Figure 2: Measured run-down signals from three vanadium ICFDs in the same vertical assembly for an SDS1 trip at PLGS.

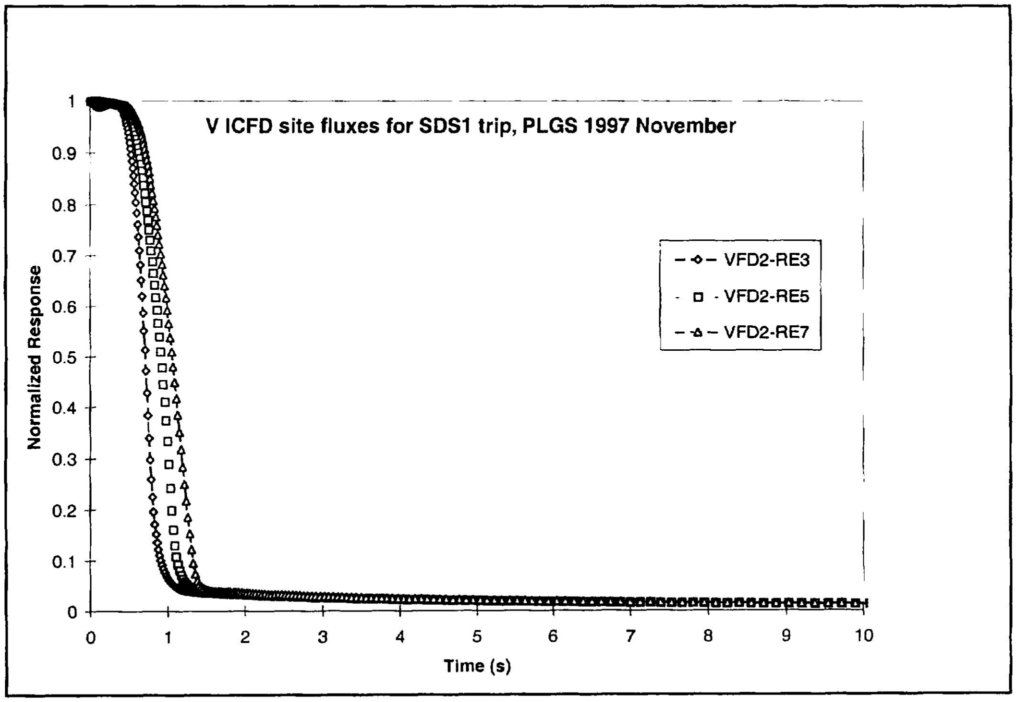

Figure 3: RFSP-simulated detector-site run-down fluxes for the three detectors shown in Figure 2.

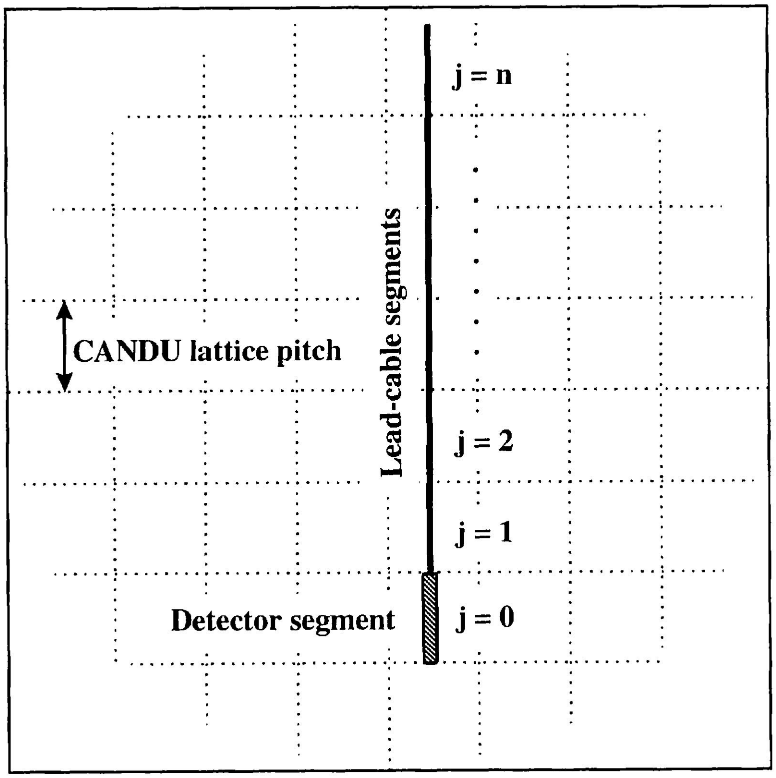

Figure 4: Schematic illustration of a vanadium ICFD and lead-cable in a CANDU reactor core.

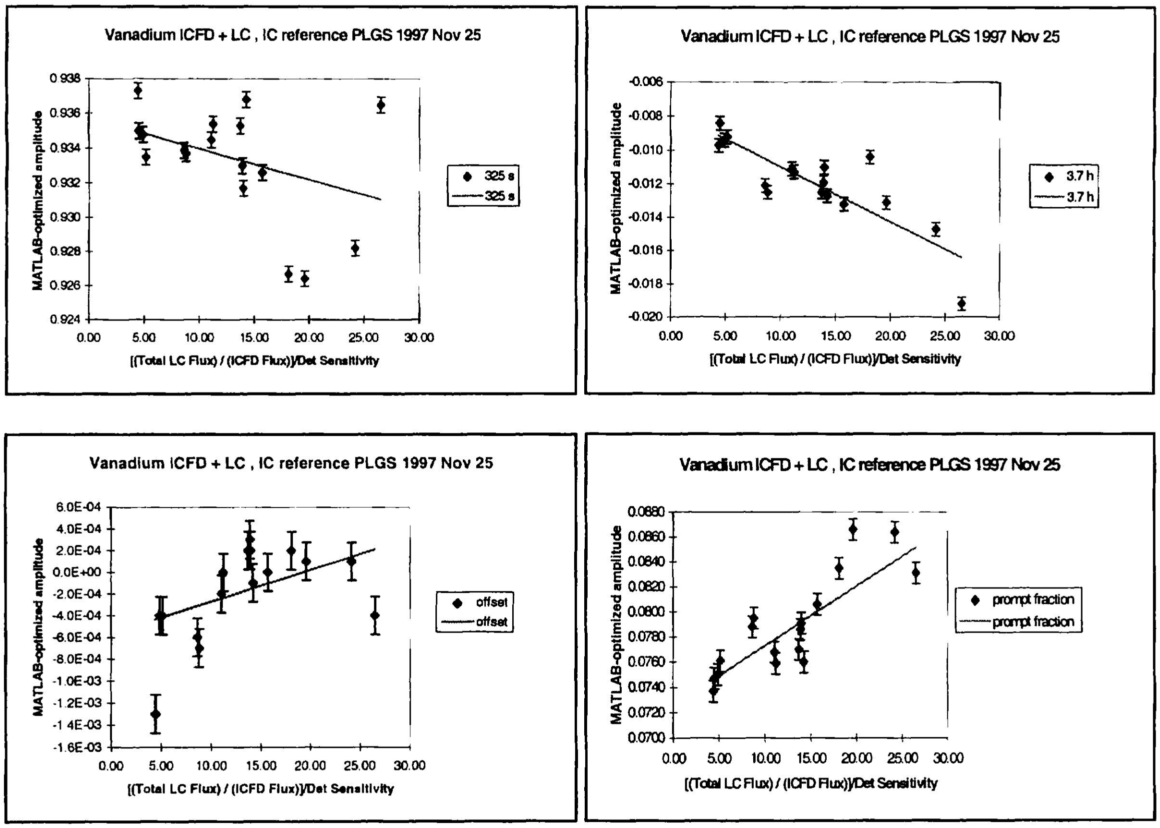

Figure 5: MDRAP-optimized amplitudes (data-points) and global best-fit (curve) vs. integrated lead-cable flux for the set of 17 vanadium ICFDs; using the IC measured response as reference.

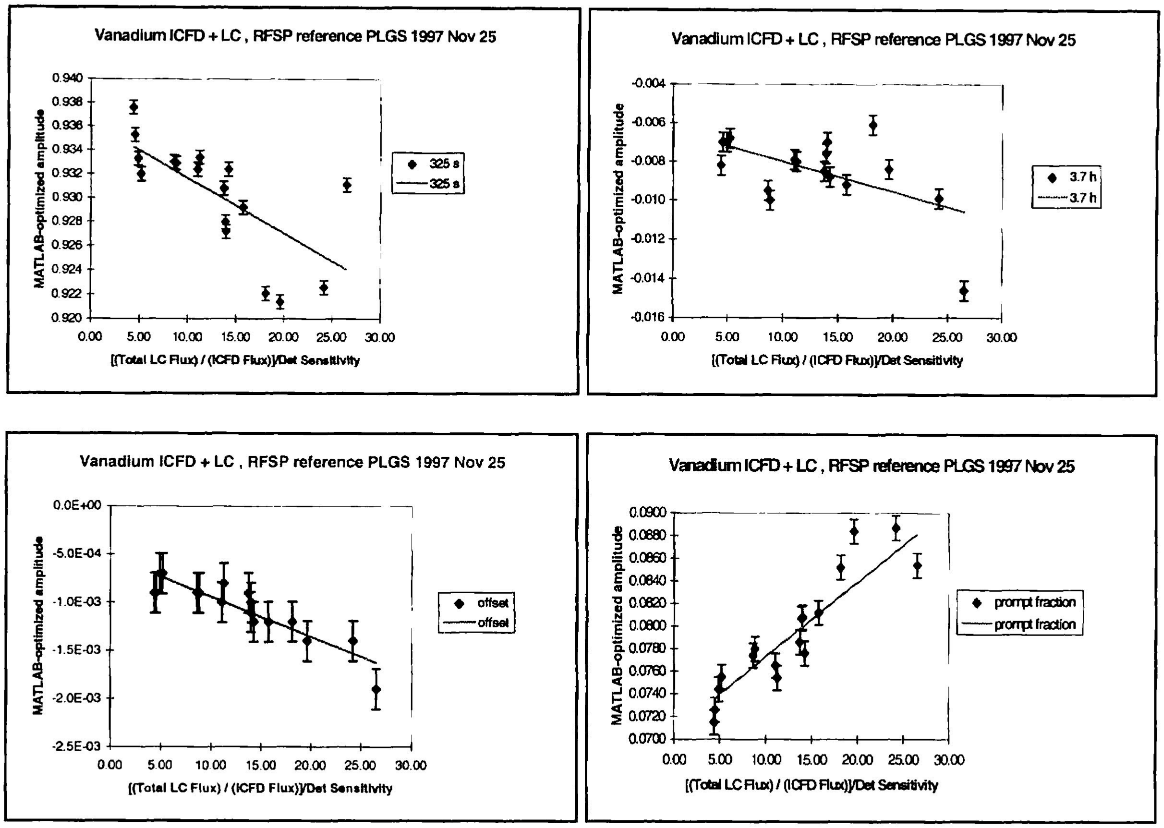

Figure 6: MDRAP-optimized amplitudes (data-points) and global best-fit (curve) vs. integrated lead-cable flux for the set of 17 vanadium ICFDs; using the RFSP-simulated detector-site fluxes as reference.

APPENDIX

Derivation of methodology to separate ICFD and lead-cable dynamic responses and to extract the lead-cable relative sensitivity.

ICFDs generate an output current in response to incident neutrons. The dynamic response of the output current with respect to time variations in the incident neutron flux may be characterized by a fractional prompt response plus the sum of a number of first order lag or exponential delay terms.

Mathematical Formulation

In the time-domain, the signal output from a single detector is:

$$I(t) = S \cdot \left[\phi(t) \cdot P + \sum_i \frac{a_i}{\tau_i} \cdot \int_{-\infty}^{t} \phi(x) \cdot e^{\frac{-(t-x)}{\tau_i}} dx \right]$$

Equation 1

where:

$I(t)$:	Output current or raw signal as a function of time
$\phi(t)$:	Flux at detector location
S:	Absolute sensitivity of detector (equilibrium output signal per unit flux)
P:	Detector prompt fraction
a_i:	Amplitude of detector dynamic response delay term i
τ_i:	time constant of detector dynamic response delay term i

and

$$P = 1 - \sum_i a_i$$

Equation 2

If the detector output has reached equilibrium with the local flux at time, t = 0, i.e., the flux has been constant or zero for a sufficient period prior to t = 0 for all delay terms to have saturated, then:

$$I(0) = S \cdot \phi(0)$$

Equation 3

and the detector output, Equation 1, can be re-written for t > 0 as:

$$I(t) = S \cdot \left[\phi(t) \cdot P + \sum_i a_i \cdot \left[\phi(0) \cdot e^{\frac{-t}{\tau_i}} + \frac{1}{\tau_i} \cdot \int_0^t \phi(x) \cdot e^{\frac{-(t-x)}{\tau_i}} \, dx \right] \right] \quad \text{(for } t>0\text{)}$$

Equation 4

The normalized response of the detector, R(t), i.e. the ratio of detector output at time t, to output at time 0, is obtained by dividing both sides of Equation 4 by Equation 3 as follows:

$$R(t) = \psi(t) \cdot P + \sum_i a_i \cdot \left[e^{\frac{-t}{\tau_i}} + \frac{1}{\tau_i} \cdot \int_0^t \psi(x) \cdot e^{\frac{-(t-x)}{\tau_i}} \, dx \right] \quad \text{(for } t>0\text{)}$$

Equation 5

where

$$R(t) = \frac{I(t)}{I(0)} \ (= 1 \text{ for } t = 0),$$

and the normalized reference flux at the detector location is

$$\psi(t) = \frac{\phi(t)}{\phi(0)} \ (= 1 \text{ for } t = 0)$$

In the frequency or s-domain, the normalized detector output, in terms of normalized reference flux is thus:

$$R(s) = \psi(s) \cdot \left(P + \sum_i \frac{a_i}{1 + s \cdot \tau_i} \right)$$

Equation 6

To make the notation compact, we note that the prompt fraction can be written as

$P = a_0$ where $\tau_0 = 0$ and $\sum_{i=0}^{5} a_i = 1$ for, say 5 delay terms. In this notation:

$$R(s) = \psi(s) \cdot \sum_{i=0}^{5} \frac{a_i}{1 + s \cdot \tau_i}$$

Equation 7

Now, consider a 1-lattice pitch long detector attached to an n-lattice pitch long in-core section of lead-cable (Figure 4). The total output will be the sum of the signals generated by the detector plus the lead-cable segments. Denote each 1-lattice pitch long segment by the subscript j, with j=0 as the detector itself. ϕ_j is the flux at the site of the segment j, and S_j is the absolute sensitivity of the detector or lead-cable segment at site j.

The total output current then is:

$$I(t) = \sum_j S_j \cdot \left[\phi_j(t) \cdot P_j + \sum_i \frac{a_{ji}}{\tau_i} \cdot \int_{-\infty}^{t} \phi_j(x) \cdot e^{\frac{-(t-x)}{\tau_i}} dx \right]$$

Equation 8

P_j is the prompt fraction of detector or lead-cable segment at site j, and a_{ji} is the amplitude, for segment j, of the lag term with time constant τ_i. For compactness of notation, a common set of time constants indexed by i is assumed for all detector and lead-cable segments. If a particular lag term, τ_l, does not appear in a particular segment, m, then its amplitude, a_{ml}, will simply be zero.

Following the development for a single detector segment (Equation 5), the normalized total output of the detector plus lead-cable segments, following equilibration of each segment output with the segment site fluxes, ϕ_j , at time t = 0, can be written as:

$$R(t) = \frac{I(t)}{I(0)} = \frac{\sum_j S_j \cdot \left[\phi_j(t) \cdot P_j + \sum_i a_{ji} \cdot \left[\phi_j(0) \cdot e^{\frac{-t}{\tau_i}} + \frac{1}{\tau_i} \cdot \int_0^t \phi_j(x) \cdot e^{\frac{-(t-x)}{\tau_i}} dx \right] \right]}{\sum_j S_j \cdot \phi_j(0)}$$

Equation 9

We note that the ratio of sensitivities of segment j to segment 0 is the definition of the lead-cable relative sensitivity, α:

$$\frac{S_j}{S_0} = \alpha_j$$

Equation 10

Next, we divide both numerator and denominator of Equation 9 by the product $S_0 \cdot \phi(0)$, and explicitly separate out the detector contribution (j = 0) from the sum of the lead cable contributions (j = 1 to n) as follows:

$$R(t) = \frac{\left[\frac{\phi_0(t)}{\phi_0(0)} \cdot P_0 + \sum_i a_{0i} \cdot \left[e^{\frac{-t}{\tau_i}} + \frac{1}{\tau_i} \cdot \int_0^t \frac{\phi_0(x)}{\phi_0(0)} \cdot e^{\frac{-(t-x)}{\tau_i}} dx\right]\right] + \sum_{j=1}^{n} \alpha_j \cdot \frac{\phi_j(0)}{\phi_0(0)} \cdot \left[\frac{\phi_j(t)}{\phi_j(0)} \cdot P_j + \sum_i a_{ji} \cdot \left[e^{\frac{-t}{\tau_i}} + \frac{1}{\tau_i} \cdot \int_0^t \frac{\phi_j(x)}{\phi_j(0)} \cdot e^{\frac{-(t-x)}{\tau_i}} dx\right]\right]}{1 + \sum_{j=1}^{n} \alpha_j \cdot \frac{\phi_j(0)}{\phi_0(0)}}$$

Equation 11

As in the case of a single detector element, we define the normalized flux at each segment site, j as:

$$\psi_j(t) = \frac{\phi_j(t)}{\phi_j(0)} \quad (= 1 \text{ for } t = 0)$$

Further we define the ratio of the segment site flux to the detector site flux at time 0 as:

$$\beta_j = \frac{\phi_j(0)}{\phi_0(0)} \quad (= 1 \text{ for } j = 0)$$

Equation 11 can be re-written as:

$$R(t) = \frac{\left[\psi_0(t) \cdot P_0 + \sum_i a_{0i} \cdot \left[e^{\frac{-t}{\tau_i}} + \frac{1}{\tau_i} \cdot \int_0^t \psi_0(x) \cdot e^{\frac{-(t-x)}{\tau_i}} dx\right]\right] + \sum_{j=1}^{n} \alpha_j \cdot \beta_j \cdot \left[\psi_j(t) \cdot P_j + \sum_i a_{ji} \cdot \left[e^{\frac{-t}{\tau_i}} + \frac{1}{\tau_i} \cdot \int_0^t \psi_j(x) \cdot e^{\frac{-(t-x)}{\tau_i}} dx\right]\right]}{1 + \sum_{j=1}^{n} \alpha_j \cdot \beta_j}$$

Equation 12

For clarity and efficiency, we write this in the compact notation of Equation 7, by noting that for each segment, including the detector segment (j = 0), the prompt fraction of the segment, $P_j = a_{j0}$ and $\tau_{j0} = 0$ and the sum rule $\sum_i a_{ji} = 1$ applies. Also, as stated previously, the relative sensitivity of the detector segment, $\alpha_0 = 1$, and the fractional flux at the detector segment site, $\beta_0 = 1$. Thus in the time domain, the normalized response is:

$$R(t) = \frac{\sum_{j=0}^{n} \alpha_j \cdot \beta_j \cdot \left[\sum_i a_{ji} \cdot \left[e^{\frac{-t}{\tau_i}} + \int_0^t \psi_j(x) \cdot e^{\frac{-(t-x)}{\tau_i}} \, dx \right] \right]}{\sum_{j=0}^{n} \alpha_j \cdot \beta_j}$$

Equation 13

and in the frequency domain, the normalized response is:

$$R(s) = \frac{\sum_{j=0}^{n} \alpha_j \cdot \beta_j \cdot \left[\psi_j(s) \right] \cdot \left(\sum_i \frac{a_{ji}}{1 + s \cdot \tau_i} \right)}{\sum_{j=0}^{n} \alpha_j \cdot \beta_j}$$

Equation 14

Assumptions and Complications

The time constants for the vanadium detector plus Inconel lead-cable are assumed to be known and fixed. They are given by the lifetime of ^{52}V - 325 s and the design value time constants of inconel SIR detectors - 95 s, 25.6 m and 3.7 h. Longer time constants are subsumed by including a signal offset term. In subsequent analyses, it may be assumed that the amplitude of the 325 s term belongs to the detector alone, since there is no vanadium present in the lead-cable material.

If the model of Equation 12, Equation 13 or Equation 14 were to be adopted at face value, then each detector simulation with n lead-cable segments would require a collection of (n+1) (for lead-cable segments plus detector) detector simulation blocks in MDRAP[6], each with its own normalized input flux, and set of delay amplitudes. This would be enormously complicated.

In practice, especially for fitting data from run-down tests, and with detector time constants of 100 s or more, such an effort is unnecessary. The *normalized* run-down curves of lattice-pitch segments from the top to the bottom of the reactor are, to first order, time-shifted from the average run-down curve, by at most ± 0.25 s (for a rod-drop or SDS1 shut down, less for a SDS2 or poison injection shut-down). Given the dominant detector time constant of 325 s, this introduces a systematic, top-to-bottom bias in the fitted amplitudes or prompt fractions of order 0.1% (= $e^{-(0.25/325)}$). It is suggested that for the sake of simplicity, this systematic error be accepted (by using a single reference flux, $\psi(s)$ for the entire detector plus lead-cable or even for the entire set of detectors plus lead-cables), and the de-convolution of detector and lead-cable effects be performed separately from the dynamic response optimization. Alternately, a first order correction can be made by using RFSP-simulated detector-site fluxes as reference fluxes for individual detectors. The RFSP-simulation accounts for SOR time-of-flight-induced flux-shape distortions at the detector sites. In any case, the de-convolution of detector and lead-cable effects cannot be performed on a detector-by-detector basis unless there is a significant difference in segment-to-segment normalized flux run-down curves (see detailed treatment below). Rather, a global, statistical analysis of the dynamic response parameters of a significant set of detectors is required.

Other complications for a global statistical analysis are listed below:

- **Burn-up** - For any given lead-cable segment, the relative sensitivity, α_j, as well as the amplitudes of individual lag terms, a_{ji}, are a function of burn-up, hence different from segment to segment. This is further complicated when comparing two different detectors because the detector sensitivity itself, S_0, depends on the individual detector burn-up. Thus two lead-cable segments, from two different detectors, may not have the same α even though they have experienced equal burn-up fluence. A first order correction for this effect can be made by computing the lead-cable relative sensitivity for segment j, α_j, as the ratio of segment sensitivity, S_j to a "standard" detector segment sensitivity, S_0. In this case, the sensitivity of the detector segment is written as $S_0 \times S_{ICFD}$. Substitution in Equation 13 or Equation 14 shows that the lead-cable flux, β_j, is corrected to (β_j / S_{ICFD}). The relative sensitivity factors of individual detectors, S_{ICFD}, are tracked as a function of burn-up. These factors, as well as the corrected lead-cable fluxes are given in Table 3.

- **Non-Linearity and In-completeness** - The relative steady-state sensitivities, α_j, and delay amplitudes, a_{ji}, may be flux dependent, instead of constant (in the short term as opposed to long-term burn-up). This results in a non-linear detector response, which is not well characterized by the linear model of Equation 1. Also, the development of the detector plus lead-cable response model, and its use in analysis pre-supposes that the response is completely specified by a set of pre-defined time-constants. Missing or wrong values of time-constants will lead to error in the dynamic response characterization, as well as in separating the detector and lead-cable responses.

- **Non-Equilibrium** - The above treatment assumes that all delayed components have equilibrated at t = 0. This assumption does not hold true, especially for the 25.6 m and 3.7 h components, when the reactor has been brought down in power a relatively short time prior to the trip. This was the case for the 1997 November 25 planned shut-down test.

Analysis Model

To simplify the analysis in the present case, the following assumptions were made:

a) All detectors have the same amplitude for each delayed term. For delay term i, this amplitude is a_{0i} (also called $a_{\text{detector } i}$ in Table 4). This assumption of uniformity in detector-to-detector dynamic response implies that burn-up dependence of detector dynamic response parameters is neglected.
b) All lead-cable segments have the same relative sensitivity, α_{LC} . (Neglect burn-up.)
c) All lead-cable segments have the same amplitude for delayed term i, a_{LCi} . (Neglect burn-up.)
d) All detector as well as lead-cable delayed terms have equilibrated prior to t = 0 for the data used in the optimization of delayed terms.

The analysis proceeds by fitting or optimizing the response of each detector to the assumed reference flux. This yields a set of detector plus lead-cable delayed amplitudes, a_i for each detector. By explicitly writing out Equation 14 with the terms defined in the above set of assumptions, we see that for each detector, the fitted amplitude is:

$$a_i = \frac{\sum_{j=0}^{n} \alpha_j \cdot \beta_j \cdot a_{ji}}{\sum_{j=0}^{n} \alpha_j \cdot \beta_j} = \frac{a_{0i} + \alpha_{LC} \cdot a_{LCi} \cdot \sum_{j=1}^{n} \beta_j}{1 + \alpha_{LC} \cdot \sum_{j=1}^{n} \beta_j}$$

Equation 15

The quantity $\sum_{j=1}^{n} \beta_j$ is the ratio of [the sum of fluxes at all lead-cable segments] to [the flux at the detector site]. This is obtained for each detector plus lead-cable from the RFSP flux-map generated just prior to the trip. We now have 17*i "data points" i.e. optimized quantities (= i detector response terms * 17 detectors) and 2*i + 1 unknown quantities (= i detector delayed terms + i lead-cable delayed terms + α_{LC}). The unknown quantities can thus be obtained by a least squares fit to the 17*i "known" quantities, subject to the constraints $\sum_i a_{0i} = 1$ and $\sum_i a_{LCi} = 1$. A further (optional) constraint is $a_{LC-325s} = 0$, i.e., an assumption that there is no vanadium-like component in the inconel lead-cable response.

A measure of the sensitivity of the analysis can be ascertained by simply plotting each amplitude a_i vs. total lead-cable relative flux, $\Sigma\beta_j$. Note from Equation 15 that if $\alpha_{LC} = 0$, then there will be no dependence of a_i on $\Sigma\beta_j$. Also to simplify the visualization, the denominator on the RHS of Equation 15 can be expanded by the binomial theorem and only leading order terms in $\alpha_{LC}\Sigma\beta_j$ retained as follows:

$$a_i = \left(a_{0i} + \alpha_{LC} \cdot a_{LCi} \cdot \sum_{j=1}^{n} \beta_j\right) \cdot \left(1 - \alpha_{LC} \cdot \sum_{j=1}^{n} \beta_j + \ldots\right) = a_{0i} + \alpha_{LC} \cdot \left(a_{LCi} - a_{0i}\right) \cdot \sum_{j=1}^{n} \beta_j + \ldots$$

Equation 16

From Equation 16, we see that if the lead-cable amplitude for a particular delayed term, a_{LCi} is assumed zero, then the plot for that particular a_i vs. $\Sigma\beta_j$ is a linear curve with intercept = the detector delayed amplitude a_{0i}, and slope = - α_{LC}*a_{0i}. This fact can be used for the ^{52}V time-constant, 325 s to act as a powerful constraint in determining α_{LC}.

The set of MDRAP-optimized amplitudes for 2 delay terms plus offset (Table 1 and Table 2) were analyzed by the above procedure. The "solver" function in Microsoft Excel was used for fitting the parameters in Equation 15 to the data (MDRAP-optimized amplitudes). The best-fit values were found by minimizing the sum of squares of error-weighted differences between the fitted and MDRAP-optimized amplitudes (i.e., χ^2). 1-σ errors in the globally-fitted amplitudes and in the lead-cable relative sensitivity were derived in the usual fashion, by (a) multiplying the errors in the amplitudes of individual detectors by a common factor so that $\chi_v{}^2{}_{min} = 1$ for the best global fit, and (b) then finding the values of the globally fitted parameters for which the otherwise unconstrained best-fit produced a value of $\chi_v{}^2{}_{min} = 2$.

The best-fit values are shown in Table 4. The global fits are illustrated in Figure 5 and Figure 6. The results are discussed in the main text of the paper.